

# **Comparison analysis between standard polysomnographic data and in-ear-EEG signals: A preliminary study**

Gianpaolo Palo<sup>1,2,†</sup>, Luigi Fiorillo<sup>1,\* †</sup>, Giuliana Monachino<sup>1,3</sup>, Michal Bechny<sup>1,3</sup>, Mark Melnykowycz<sup>4</sup>, Athina Tzovara<sup>3</sup>, Valentina Agostini<sup>2</sup>, and Francesca Dalia Faraci<sup>1</sup>

<sup>1</sup>Institute of Digital Technologies for Personalized Healthcare (MeDiTech), Department of Innovative Technologies, University of Applied Sciences and Arts of Southern Switzerland, Lugano, Switzerland; <sup>2</sup>Department of Electronics and Telecommunications, Politecnico di Torino, Torino, Italy; <sup>3</sup>Institute of Computer Science, University of Bern, Bern, Switzerland; <sup>4</sup>IDUN Technologies AG, Glattpark, Switzerland.

Institution where work was performed: Institute of Digital Technologies for Personalized Healthcare (MeDiTech), Department of Innovative Technologies, University of Applied Sciences and Arts of Southern Switzerland, Lugano, Switzerland.

†These authors contributed equally to this work.

\*Corresponding author. Luigi Fiorillo, Institute of Digital Technologies for Personalized Healthcare (MeDiTech), Department of Innovative Technologies, University of Applied Sciences and Arts of Southern Switzerland, Lugano, Switzerland. Email:

[luigi.fiorillo@supsi.ch](mailto:luigi.fiorillo@supsi.ch).

## Abstract

**Study Objectives:** Polysomnography (PSG) currently serves as the benchmark for evaluating sleep disorders. Its discomfort makes long-term monitoring unfeasible, leading to bias in sleep quality assessment. Hence, less invasive, cost-effective, and portable alternatives need to be explored. One promising contender is the in-ear-EEG sensor, which offers advantages in terms of comfort, fixed electrode positions, resistance to electromagnetic interference, and user-friendliness. This study aims to establish a methodology to assess the similarity between the in-ear-EEG signal and standard PSG.

**Methods:** We assess the agreement between the PSG and in-ear-EEG derived hypnograms. We extract features in the time- and frequency- domain from PSG and in-ear-EEG 30-second epochs. We only consider the epochs where the PSG-scorers and the in-ear-EEG-scorers were in agreement. We introduce a methodology to quantify the similarity between PSG derivations and the single-channel in-ear-EEG. The approach relies on a comparison of distributions of selected features - extracted for each sleep stage and subject on both PSG and the in-ear-EEG signals - via a Jensen-Shannon Divergence Feature-based Similarity Index (JSD-FSI).

**Results:** We found a high intra-scorer variability, mainly due to the uncertainty the scorers had in evaluating the in-ear-EEG signals. We show that the similarity between PSG and in-ear-EEG signals is high (JSD-FSI:  $0.61 \pm 0.06$  -awake,  $0.60 \pm 0.07$  -NREM and  $0.51 \pm 0.08$  -REM), and in line with the similarity values computed independently on standard PSG-channel-combinations.

**Conclusions:** In-ear-EEG is a valuable solution for home-based sleep monitoring, however further studies with a larger and more heterogeneous dataset are needed.

**Keywords:** sleep wearables, in-ear-EEG, machine learning, sleep staging, multi-source-scored sleep databases.

## **Statement of Significance**

Whole Polysomnography may prevent from depicting real sleep patterns due to the extensive setting employed. An alternative to overcome this limitation is to use wearable solutions like the in-ear-EEG. To date, the in-ear-EEG and the standard PSG derivations have only been compared following basic correlation analysis. We propose a more exhaustive methodology - hypnogram-based and feature-based - to evaluate the similarity between the in-ear-EEG and PSG signals. The ultimate goal is to investigate whether in-ear-EEG sensors inherit information close to the ones we extract through standard PSG.

## Introduction

Polysomnography (PSG) is the gold standard to perform sleep studies [1-3]. PSG is performed in appropriate clinical facilities, and involves recording multiple bio-signals during a full night's sleep, including brain activity (EEG), eye movements (EOG), muscle activity (EMG), cardiac activity (ECG), body position, breathing effort, blood saturation, etc. The PSG recordings are nowadays manually evaluated by trained personnel according to the American Academy of Sleep Medicine (AASM) manual [4]. Despite being highly standardized by AASM guidelines, this manual procedure is time- and effort- consuming, and it is not error-free [5]. These limitations, along with the saturation of the sleep units, lead to high costs related to patient management and care. Besides, due to the invasive equipment, and since the patients are typically sleeping in an atypical and unfamiliar environment, standard PSG-based analyses introduce biases to the sleep quality assessment [1, 2].

Wearable and portable devices may be valid solutions, as they allow for home-based sleep monitoring. The use of unconventional channels has been widely explored in the field of mobile sleep monitoring with wearable devices. [6] provides a comprehensive overview about sensing technologies (different signals and their combinations) for sleep staging via wearable devices. The signals conveying a substantial amount of information for this task are EEG, EOG, and EMG - with the EEG signal being the most used sensing modality as a single data source. We might therefore speculate that ear-EEG may be the right choice. The brain activity is recorded from electrodes placed in or around the ear, while also leading to several advantages in comfort, fixed electrode positions, robustness to electromagnetic interference, and ease of use [1, 7].

To date, only two research groups have exploited ear-EEG signals for sleep analysis. The majority of their studies mainly relied on feature-based methodologies to evaluate the

feasibility of ear-EEG technology for automated sleep monitoring. They showed that automatic sleep scoring based on ear-EEG signals was performing at levels comparable to expert scoring of PSG, in young healthy subjects [2, 8-13].

Jørgensen et al. [14] study can be seen as a proof of concept for the suitability of ear-EEG on epileptic subjects and in [15], Kjaer et al. showed that sleep metrics computed from multiple nights automatically scored on ear-EEG are more reliable than the ones computed from a single night manually scored via standard PSG. Thus, highlighting how ear-EEG seems to be a useful alternative for sleep staging for the single night recording, and an advantageous choice for several nights of sleep monitoring.

However, in none of the above mentioned studies - even before inferring and/or validating sleep metrics and/or algorithms on these promising signals - the similarity between each standard PSG and the ear-EEG derivations has been thoroughly investigated or quantified.

In this work, we carried out the above mentioned comparison analysis, first focusing on the sleep scoring procedure (*hypnogram-based*), then directly evaluating the signals (*feature-based*). The hypnogram-based comparison analysis is performed assessing the agreement (i.e., Cohen's kappa) between the PSG and in-ear-EEG derived hypnograms. Specifically, quantifying the inter- and intra- scorer variability on the multi-source-scored database. Whilst, the feature-based comparison analysis is conducted extracting time- and frequency- domain features, as to quantify the similarity between standard PSG derivations and recordings coming from a single-channel in-ear-EEG earbuds sensor. In-ear-EEG sensors are thought to perform better - for sleep scoring tasks - when combined with additional EOG signals [3, 16] - especially in distinguishing REM sleep stage. Thus, we extract features from both EOG and scalp-EEG derivations (i.e., frontal, central and occipital brain regions), to then compare them to features extracted from the in-ear-EEG sensor. Among the scalp-EEG derivations we also included the mastoid-to-mastoid one (M1-M2), as its information has been proven to be similar to the in-ear-EEG [7, 11].

The proposed approach relies on a comparison of the distributions of the selected features - extracted from the two different sources, PSG and in-ear-EEG respectively - via the newly introduced Jensen–Shannon Divergence Feature-based Similarity Index (JSD-FSI).

In the present work we investigate whether or not in-ear-EEG sensors inherit information - or set of features - close to what we usually extrapolate through standard PSG derivations. In particular: (1) we found a high intra-scorer variability (PSG versus in-ear-EEG scoring), mainly due to the great uncertainty the scorers had in evaluating the in-ear-EEG signals; (2) we show that the similarity between the PSG and the in-ear-EEG signals - in terms of JSD-FSI score - is high, on average  $0.61 \pm 0.06$  in awake,  $0.60 \pm 0.07$  in NREM and  $0.51 \pm 0.08$  in REM; (3) we demonstrate that the spatial distributions of the JSD-FSI scores (any pair in-ear-EEG and PSG derivations) is on average consistent within the different subjects and channels; significant changes in JSD-FSI scores are found between awake and REM ( $p$ -value  $< 0.001$ ) and between NREM and REM stages ( $p$ -value  $< 0.001$ ), whilst no significant change is found between awake and NREM stages ( $p$ -value  $> 0.05$ ); (4) we prove that the JSD-FSI similarity values reported in (2) are in line with the similarity values computed independently on the different combinations of PSG channels - further testifying the overlap between the two different sources.

## Methods

We exploit an already existing dataset collected during an observational study carried out at IDUN Technologies. In the hypnogram-based comparison analysis, we describe how to compute the consensus in the multi-source-scored dataset (i.e., a dataset where each recording is scored by multiple experts and looking at different sources of signals).

Establishing a consensus is crucial at first to be able to quantify the inter- and intra- scorer variability on the two different sources, then to simplify the feature-based comparison

analysis - i.e., analyzing only the sleep epochs where the PSG-scorers and the in-ear-EEG-scorers were in agreement on the associated sleep period.

Indeed, in our feature-based comparison procedure we evaluate the similarity between the signals coming from two different sources for each sleep stage independently. The feature-based analysis is divided in three steps: feature extraction (time- and frequency-domain features), feature selection, and definition of a Jensen-Shannon Divergence (JSD) - Feature-based Similarity Index (FSI).

## Dataset

The clinical study (BASEC Nr. Req-2022-00105) involves 10 healthy subjects, including both females and males (18-60 years) selected according to the Pittsburgh sleep quality index (PSQI) [17]. Following a screening period of 28 days, the subjects experience one overnight stay at the investigational site. Participants are monitored using multiple standard surface electrodes on their scalp (EEG), outer canthus of each eye (EOG), mentalis (chin), torso (EKG) in the conventional PSG monitoring, and an additional in-ear-EEG sensing technology monitoring. Participants arrive approximately three hours prior to their normal bedtime at the sleep laboratory, and they are instructed about the overall structure of the study, including PSG preparation /setting phase, a sleep restriction phase  $\approx$  4 hours, and the sleep phase  $\approx$  4 hours ([Figure 1](#)).

The subjects are asked to avoid caffeine intake from noon before arriving at the study center. They perform specific head and eye movements for bio-calibrating the instrumentation used for data collection. The sleep restriction starts at the in-bed time of each subject and lasts for about four hours, after which participants are allowed to sleep for another four hours. During the last hour of the sleep restriction phase, the subjects abstain from using electronic devices. The sleep room is set up according to AASM guidelines [4]. The Karolinska Sleepiness Scale (KSS) [18] is administered at the beginning and at the end of the sleep restriction period, and prior to sleep to assess subjective drowsiness.

PSG and in-ear-EEG signals are recorded simultaneously. The data analyzed in this study refer only to the four hours recorded during the sleep phase.

PSG signals are collected using a SOMNOmedics SOMNOscreen plus system with a sampling frequency of 256 Hz ([Figure 2a](#)). The signals are band-pass filtered between 0.2-35 Hz and ECG artifacts removed. A total of 21 channels are investigated, considering both bipolar and unipolar derivations: two reference electrodes (M1, M2); six EEG bipolar derivations (C3-M2, F3-M2, O1-M2, C4-M1, F4-M1, O2-M1); six EEG unipolar derivations (C3, C4, F3, F4, O1, O2); four EOG bipolar derivations (E1-M1, E1-M2, E2-M1, E2-M2); two EOG unipolar derivations (E1, E2); the mastoid-to-mastoid derivation (M2-M1). From here on, we will refer to the set of PSG channels as the set  $Q$ .

In-ear-EEG signals are collected via the GDK (Guardian Development Kit) device designed by IDUN Technology with a sampling frequency of 250 Hz ([Figure 2b](#)). The signals are band-pass filtered between 0.5-35 Hz, before being normalized as their amplitude range would match the one of the simultaneously recorded PSG signals. In-ear-EEG recordings are multiplied with the standard deviation ratio of PSG and in-ear-EEG data. From here on, we will refer to the single in-ear-EEG channel as CH1 channel.

PSG and in-ear-EEG signals are manually synchronized based on easily distinguishable artifacts in both data streams. They are then trimmed such that the recordings referring to the same subject share the same length.

Three scorer experts separately score both PSG and in-ear-EEG data, according to AASM guidelines [4]. The dataset contains the following annotations W, N1, N2, N3, REM, MOVEMENT and UNKNOWN, where the last two refer respectively to movement artifacts



and to no sleep stage assigned. In this study, the three non-REM sleep stages are combined together under the label NREM.

## Comparison analysis: hypnogram-based approach

### Consensus in a multi-source-scored dataset

In the hypnogram-based approach, in order to quantify the inter- and intra- scorer variability on the two different sources, we compute the consensus among the three scorers on each data source - inspired by previous studies [19, 20] analyzing multi-scored databases. The majority vote from the scorers has been computed - i.e., we assign to each 30-second epoch the most voted sleep stage among the scorers. In case of ties, we compute the soft-agreement metric [20] to then consider the label from the most reliable scorer. The most reliable scorer is the one that is frequently in agreement with all the others. We rank the reliability of each scorer, to finally define the most reliable scorer, for each subject.

We denote with  $J$  the total number of scorers and with  $j$  the single-scorer. The one-hot encoded sleep stages given by the scorer  $j$  are:  $\hat{y}_j \in [0, 1]^{K \times T}$ , i.e., 1 assigned for the scored stage and 0 for the other stages,  $K$  is the number of classes, i.e.,  $K = 3$  sleep stages, and  $T$  is the total number of epochs. The probabilistic consensus  $\hat{z}_j$  among the  $J - 1$  scorers ( $j$  excluded) is computed using the following:

$$\hat{z}_j = \frac{\sum_{i=1}^J \hat{y}_i[t]}{\max_j \sum_{i=1}^J \hat{y}_i[t]} \quad \forall t; \quad i \neq j \quad (1)$$

where  $t$  is the  $t$ -th epoch of  $T$  epochs and  $\hat{z}_j \in [0, 1]^{K \times T}$ , i.e., 1 is assigned to a stage if it matches the majority or if it is involved in a tie. The *Soft-Agreement* is then computed separately for each scorer across all the  $T$  epochs as:

$$Soft-Agreement_j = \frac{1}{T} \sum_{t=0}^T \hat{z}_j[y_j] \quad (2)$$

where  $\hat{z}_j[y_j]$  denotes the probabilistic consensus of the sleep stage chosen by the scorer  $j$  for the  $t$ -th epoch.  $Soft-Agreement_j \in [0, 1]$ , where the zero value is assigned if the scorer  $j$  systematically scores all the annotations incorrectly compared to the others, whilst 1 is assigned if the scorer  $j$  is always involved in tie cases or in the majority vote. The *Soft-Agreement* is computed for all the scorers, and the values are sorted from the highest - high reliability - to the lowest - low reliability.

The *Soft-Agreement* is computed for each subject, i.e., the scorers are ranked accordingly, and in case of a tie the top-1 scorer will be the one used for that subject. In Supplementary Table S1 and Table S2 we report the *Soft-Agreement* values computed on each of three scorers, and for each subject, on the PSG and in-ear-EEG data sources respectively.

In the feature-based comparison analysis we define similarity-scores between the two different data sources, PSG and in-ear-EEG, exploiting a per-sleep-stage-based approach. Hence, we first define a common label-ground-truth reference for both types of signal, to prevent additional bias in our analysis. Only the epochs scored in the same sleep stage by both the computed consensus, i.e., PSG and in-ear-EEG based scoring procedures, are included. In [Table 1](#) we report a summary of the total number and percentage of the epochs per sleep stage for both PSG and in-ear-EEG based scoring procedure, and the intersection ( $n$ ) computed on the labels coming from the two different sources.

## Comparison analysis: feature-based approach

In order to assess the similarity between standard PSG and in-ear-EEG signals we follow specific steps (as summarized in [Figure 3a](#)): (1) we extract time- and frequency- domain

features from the above-mentioned PSG derivations and the in-ear-EEG channel on each 30-second sleep epoch; (2) we remove all redundant features through pairwise assessments (feature selection procedure) to identify those conveying the same information; (3) we then define the JSD - Feature based Similarity Index (FSI) exploited to compare the distributions of the selected features, for each sleep stage and for each subject on both PSG derivations and the in-ear-EEG.

To fairly validate the results of our comparison analysis, we decided to also quantify the similarity between all the possible combinations of PSG derived signals, including scalp-EEG and EOG channels ([Figure 3b](#)). The idea is to assess that the PSG-to-In-ear JSD-FSI similarity-scores (histograms in blue [Figure 3a](#)) are on average close to those derived from the standard PSG-to-PSG comparisons (histograms in red [Figure 3b](#)). The results are evaluated separately for each sleep stage and for each subject.

## Feature extraction

We extract both time- and frequency- domain features from 30-second epochs of signals. All the features depending on the amplitude are computed on signals normalized by their maxima, compensating for differences in magnitudes.

### Time-domain features

First we simply compute standard descriptive statistics (e.g., mean, standard deviation, interquartile range, skewness, kurtosis, etc..), the maximum first derivative and the number of zero-crossings. We then include entropy based measures, specifically, the approximate entropy [22-24], the sample entropy [22-26], the singular value decomposition (SVD) entropy [25, 26], and the permutation entropy [25, 27]. To assess the complexity of the signals we consider the Lempel-Ziv complexity [28] and the detrended fluctuation analysis (DFA) exponent [29, 30]. In addition, we also include Hjorth parameters of activity, mobility, and

complexity [31], the Katz, Higuchi [32] and Petrosian [33] fractal dimensions [34, 35] to further quantify the complexity or irregularity of the analyzed time series.

In Supplementary Analyses we report additional mathematical details for each of the above features.

### Frequency-domain features

We first compute the power spectral density (PSD) of each 30-second signal using the Welch's average periodogram method [36]. We choose a Hamming window of 5-second length with a 50% overlap, resulting in a frequency resolution of 0.2 Hz [30, 37]. We exploited the Hamming window to reduce the estimation variance, the side-lobe effect and the spectral leakage phenomena [38]. The 5-second window length is set to be at least twice the lowest frequency of interest 0.5 Hz (i.e., the lower end of the EEG delta power band) [37]. Then, the median-average partially mitigates the influence of any noise/artifacts we have on our signals [30, 37].

Once the PSD has been computed, we first extract standard frequency-domain features, such as the spectral energy of the whole 30-second signal, and the relative spectral power on all the EEG frequency bands, i.e., delta ( $\delta$ , 0.5–4 Hz), theta ( $\theta$ , 4–8 Hz), alpha ( $\alpha$ , 8–12 Hz), sigma ( $\sigma$ , 12–16 Hz), beta ( $\beta$ , 16–30 Hz), and gamma ( $\gamma$ , 30–35 Hz). We then include several ratio measures between the different frequency bands, i.e.,  $\delta/\theta$ ,  $\delta/\sigma$ ,  $\delta/\beta$ ,  $\theta/\alpha$ ,  $\delta/\alpha$ ,  $\alpha/\beta$ ,  $\delta/(\alpha + \beta)$ ,  $\theta/(\alpha + \beta)$ , and  $\delta/(\alpha + \beta + \theta)$ .

In our frequency domain analysis, we include additional features assessing the spread, symmetry, tail behavior, shape and complexity of each 30-second signal's spectrum distribution. Specifically, we compute the four central moments in statistics (i.e., mean, variance, skewness, and kurtosis), the spectral entropy and the Renyi entropy [39], the

spectral centroid [40, 41], the spectral crest factor [42], the spectral flatness [40, 41], the spectral roll-off [43], and the spectral spread [41].

In Supplementary Analyses we report the complete list of all the time- and frequency-domain features extracted (Table S3 and Table S4) and additional mathematical details for each of the above features.

### Feature selection

The feature selection procedure is essential to remove in our analysis possible redundancy within the feature subset. We exploit a feature selection algorithm based on pairwise feature correlation [44, 45], aiming to identify the most representative features among all the extracted ones. However, before proceeding with this procedure, we should first consider that the above derived features are meant to describe the morphology of our neurological signals. The features are all supposed to change based on the state brain subjects are in, i.e., waking state, NREM state or REM state. Thus, we decide to first divide the data, i.e., the 30-second epochs, depending on the sleep stage they are assigned to.

Therefore, for each pair of channels (i.e., a pair is defined as  $\{q, CH1\}$ , where  $q \in Q$ , and  $Q$  is the above defined set of PSG channels), we build pairs of datasets  $\{D^q, D^{CH1}\}$ , one pair for each of the  $k \in K$  sleep stages. Each dataset  $D \in \mathfrak{R}^{M \times N \times K}$  is the result of concatenated feature vectors  $\bar{f}_{n,k}$ , where  $K = 3$  is the number of sleep stages,  $N$  is the total number of features, with  $n \in N$ , and  $M$  is the total number of 30-second epochs in each stage.

A z-score normalization is performed separately on each dataset-pair,  $D^q$  and  $D^{CH1}$ , and for each sleep stage, to reduce dissimilarities among the different subjects. On each dataset, we perform the feature selection based on the computation of a modified version of the maximal information compression index (MICI) between each pair of features [44-46]. As the

algorithm adopts a k-nearest neighbors approach, the determination of the initial k value is crucial and is guided by metrics such as the representation entropy [44, 45] and the redundancy rate [45, 47].

In Supplementary Analyses we report additional mathematical details regarding the modified version of the feature selection algorithm, along with further details on the k-nearest neighbors approach.

### JSD - Feature based Similarity Index (JSD-FSI)

We quantify the similarity between pairs of feature distributions, coming from two different sources (e.g., PSG derived and in-ear-EEG derived), exploiting the Jensen-Shannon Divergence (JSD) [48]. The JSD divergence is a symmetric and smoothed version of the Kullback-Leibler (KL) divergence [49], quantifying the similarity between two probability distributions. Practically, we first compute the probability density function (PDF)  $\Phi$  for each pair of feature distributions  $\{\Phi(\bar{f}_{n,k}^q), \Phi(\bar{f}_{n,k}^{CH1})\}$  extracted from the paired datasets  $\{D^q, D^{CH1}\}$  [50]. We then measure the dissimilarities between each pair via the JSD divergence. JSD ranges from 0 (identical distributions) to 1 (completely dissimilar distributions). The higher the number, the more dissimilar the probability distributions.

Hence, once we compute the JSD metric on each PDF feature pair  $\{\Phi(\bar{f}_{n,k}^q), \Phi(\bar{f}_{n,k}^{CH1})\}$ , for each sleep stage  $k$  and of each subject, we can finally compute the JSD Feature based Similarity Index (*JSD-FSI*) between each PSG  $q$  channel and the in-ear-EEG  $CH1$  channel as follows:

$$JSD-FSI_{k \in K} = \sum_{n=1}^N (1 - JSD_n) / N \quad (3)$$

$$JSD_n(\Phi(\bar{f}_{n,k}^q) \parallel \Phi(\bar{f}_{n,k}^{CH1})) = \left( KL(\Phi(\bar{f}_{n,k}^q) \parallel M) + KL(\Phi(\bar{f}_{n,k}^{CH1}) \parallel M) \right) / 2 \quad (4)$$

where  $N$  is the total number of features,  $M$  is the *average* distribution defined as

$M = \left( \Phi(\bar{f}_{n,k}^q) + \Phi(\bar{f}_{n,k}^{CH1}) \right) / 2$ , whilst  $KL(\Phi(\bar{f}_{n,k}^q) \parallel M)$  is the Kullback-Leibler divergence

between the two distributions  $\Phi(\bar{f}_{n,k}^q)$  and  $M$ , defined as:

$$KL(\Phi(\bar{f}_{n,k}^q) \parallel M) = \sum f_k^q(t) * \log(f_k^q(t) / M(t)) \quad \forall t; \quad (5)$$

Hence, for each sleep stage and for each subject, we derive 21 (i.e., simply the total number of pairs comparisons  $\{q, CH1\}$ ) *JSD-FSI* similarity-scores. Each of these scores is defined as the sum of the individual  $JSD_n$  similarity-scores - resulting from all the PDF feature distributions comparisons - divided by the total number of features analyzed (2).

The same comparison analysis has been done between all the possible combinations of PSG derived signals, i.e., scalp-to-scalp, scalp-to-EOG, and EOG-to-EOG comparisons. We compare all the PDF feature distributions extracted from all the channels in the PSG set  $Q$  (unique comparisons, i.e., upper triangle of the symmetric matrix with dimension  $(|Q| \times |Q|)$ , where  $|Q| = 21$  is the cardinality of the set, or the total number of PSG channels).

Hence, we first compute the probability density function (PDF)  $\Phi$  for each pair of feature distributions  $\{\Phi(\bar{f}_{n,k}^{q_i}), \Phi(\bar{f}_{n,k}^{q_j})\}$  extracted from the dataset pairs  $\{D^{q_i}, D^{q_j}\}$ , with  $i \neq j$ . We then compute the *JSD-FSI* similarity-scores on all the possible combinations as described above. In that case, for each sleep stage and for each subject, we derive 210 (i.e., unique comparisons between all the PSG channels via the binomial coefficient  $\frac{|Q|!}{2!(|Q|-2)!}$ ) *JSD-FSI* similarity-scores.

We will fairly assess, for each sleep stage and for each subject, that the PSG-to-In-ear JSD-FSI similarity-scores are on average close to those derived from the standard PSG-to-PSG comparisons.

## Results

### Comparison analysis: hypnogram-based approach

#### Intra- and inter- scorer variability in the multi-source-scored dataset

When assessing the *Soft-Agreement* metric - hence the PSG and the in-ear-EEG consensus - it is clear that the in-ear-EEG scorers consistently yield lower values compared to PSG scorers (see Table S1 and Table S2), i.e., limited agreement among the in-ear-EEG scorers. To further validate this observation, we compute the Cohen's kappa metric ( $\kappa$ ) [21]. Cohen's kappa metric ranges from  $-1$  (indicating entirely disagreement) to  $+1$  (representing perfect matching). A value of 0 suggests random agreement among raters. We measure  $\kappa$  between each pair of PSG and in-ear-EEG hypnograms referring to the same recording/subject scored by the same scorer expert.

In [Figure 4](#) we report, for each scorer, the distribution of the kappa values computed for each recording/subject between the PSG and in-ear-EEG hypnograms - so quantifying the intra-scorer variability in the multi-source-scored dataset. In this context, the  $\kappa$  values exhibit considerable dispersion across all distributions, with limited agreement levels, particularly in the comparison performed on the scorer 2.

Subsequently, we assess Cohen's kappa values by comparing hypnograms from the same recording/subject, scored by the three expert scorers, first on PSG and then on in-ear-EEG signals - so quantifying the inter-scorer variability in the multi-source-scored dataset ([Figure 5](#)). Notably, the kappa intervals among PSG scorers exhibit greater coherence and



consistency compared to those for in-ear-EEG scorers. This is evident in the reduced dispersion and higher average values observed in PSG scorer comparisons.

## Comparison analysis: feature-based

### JSD-FSI similarity-scores

The most frequently selected features across the different datasets  $\{D^q, D^{CH1}\}$  for all the three sleep stages ([Figure 6](#)) are the following: the relative  $\delta$ ,  $\theta$ ,  $\alpha$ , and  $\sigma$  power bands; the  $\theta/\alpha$  and  $\alpha/\beta$  power ratios; the spectral flatness; the skewness; the kurtosis; the maximum first derivative; and the Hjorth complexity. In addition, there are extra selected features specifically for each sleep stage: the  $\delta/\theta$ ,  $\delta/\sigma$  power ratios, the permutation entropy, the DFA exponent and the Higuchi fractal dimension for the awake stage; the relative  $\beta$  and  $\gamma$  power bands, the spectral skewness, the spectral roll-off, the standard deviation, and the Hjorth activity for the NREM sleep stage; and the relative  $\gamma$  power band, the  $\delta/\alpha$  power ratio, and the standard deviation for the REM sleep stage. Bear in mind that the above selected features are not to be understood as more or less relevant to the purpose of our comparison analysis. The not-selected features were ignored simply because of the redundant information they were bringing.

In [Figure 7](#), [Figure 8](#) and [Figure 9](#) we report the JSD-FSI similarity-scores computed between the in-ear-EEG and PSG channels - for each sleep stage respectively - in standard topographic images. Overall, the similarity between the PSG and the in-ear-EEG signals - in terms of JSD-FSI score - is high, on average  $0.61 \pm 0.06$  in awake,  $0.60 \pm 0.07$  in NREM and  $0.51 \pm 0.08$  in REM. Across all subjects there are no substantial differences with the in-ear-EEG compared to the corresponding PSG channel. The spatial distributions in terms of JSD-FSI scores (any pair in-ear-EEG and PSG derivations) is on average consistent within the different subjects and channels. According to Mann-Whitney U-test ( $\alpha = 0.05$ ), significant changes in JSD-FSI scores are found between awake and REM stages (p-value <

0.001) and between NREM and REM stages ( $p$ -value  $< 0.001$ ), whilst no significant change is found between awake and NREM stages ( $p$ -value  $> 0.05$ ). In detail, there is statistical evidence in the awake stage ( $p$ -value  $< 0.001$ ) and in the NREM stage ( $p$ -value  $< 0.001$ ) that JSD-FSI similarity scores are greater than REM ones. A non-parametric statistical test is used as the normality assumption is not met based on the Shapiro-Wilk test ( $\alpha = 0.05$ ).

When assessing the similarity between in-ear-EEG and PSG derivations, and comparing it to the similarity computed among all the possible 210 PSG-to-PSG comparisons (JSD-FSI similarity-scores computed from the PSG channels), similar values are observed. In [Figure 10](#), [Figure 11](#) and [Figure 12](#) we show that, for every sleep stage, the blue distributions (i.e., JSD-FSI similarity-scores from the PSG-to-In-ear comparisons) consistently align with the red ones (i.e., JSD-FSI similarity-scores from the PSG-to-PSG comparisons). Even in cases where there is no complete or partial overlap, there are still moderate similarity scores, with values surpassing a threshold of 40%.

## Discussion

While evaluating the agreement between the PSG and in-ear-EEG hypnograms scored by the same scorer expert (hypnogram-based comparison analysis), we found a high intra-scorer variability. The high variability - or inconsistency between the two different sources - is mainly due to the great uncertainty the scorers had in evaluating the in-ear-EEG signals (see the inter-score variability analysis). The  $\kappa$  values between pairs of in-ear-EEG scorers are on average lower - and not consistent - compared to the ones computed on the PSG scorers. We may infer that the in-ear-EEG recordings are clearly harder to score than traditional PSG signals. Nevertheless, this heightened scoring complexity may not stem from the substandard quality of the in-ear EEG signal, but rather from the innovative nature of the EEG source captured from our ears - distinctly divergent from what scoring experts are used to look at.

Indeed, the main outcome of the feature-based comparison analysis is that there is actually a substantial similarity in terms of JSD-FSI score - on average  $0.61 \pm 0.06$  in awake,  $0.60 \pm 0.07$  in NREM and  $0.51 \pm 0.08$  in REM - between the two different sources. The in-ear-EEG signals are retaining information (in time- and frequency- domain) close to the ones we usually extrapolate through standard PSG derivations. This latter claim is in contrast to what we found via the previous hypnogram-based comparison analysis, which was mainly relying on the knowledge and the taste of the scoring experts.

However, significant changes in JSD-FSI scores are found between awake and REM, and between NREM and REM stages. These results are in line with what we already knew to date: the in-ear-EEG sensors may be not enough in distinguishing REM sleep stage - additional information from EOG signals are needed.

The robustness of the JSD-FSI similarity scores mentioned above - and the significance of the similarity values per se - is further validated showing the clear overlap between the PSG-to-In-ear-EEG and PSG-to-PSG JSD-FSI score distributions. The similarity between the in-ear-EEG and any PSG derivation is close to the similarity we would find between any pair of standard scalp PSG derivations.

The main limitation of our preliminary work is that we cannot make any comprehensive consideration regarding JSD-FSI consistency between subjects or channels - i.e., spatial distribution. There is a need to further validate the proposed methodology on a higher number of recordings - eventually involving subjects affected by different sleep disorders - i.e., data heterogeneity.

## Funding

The present work has been partially funded by IDUN GESSE (Guardian Earbuds Sleep Scorer Expert), INNO-ICT 65141.1, from the Innovation Cheque funding program.

## Conflict of Interest

SUPSI authors are responsible for the research, and they conducted the analysis independently. IDUN Company representative contribution was in offering detailed information about the device and the dataset collected in a previous study.

## Data availability

The dataset from IDUN (BASEC Nr. Req-2022-00105) is not publicly available. The data are available on request from the corresponding author L.F., for non-commercial purposes only and after complying to IDUN's ethics guidelines (legal conditions ensuring data privacy will be defined in a “data transfer agreement document”, together with a description of the analysis project).

## References

- [1] Stochholm A, Mikkelsen K, and Kidmose P. Automatic sleep stage classification using ear-EEG. 2016 38th Annual International Conference of the IEEE Engineering in Medicine and Biology Society (EMBC). IEEE. 2016 :4751–4. doi: 10.1109/EMBC.2016.7591789.
- [2] Tabar YR, Mikkelsen KB, Shenton N, Kappel SL, Bertelsen AR, Nikbakht R, Toft HO, Henriksen CH, Hemmsen MC, Rank ML, et al. At-home sleep monitoring using generic ear-EEG. *Frontiers in Neuroscience* 2023; 17:987578. doi: 10.3389/fnins.2023.987578.

- [3] Zibrandtsen I, Kidmose P, Otto M, Ibsen J, and Kjaer T. Case comparison of sleep features from ear-EEG and scalp-EEG. *Sleep Science* 2016; 9:69–72. doi: 10.1016/j.slsci.2016.05.006.
- [4] Berry RB, Brooks R, Gamaldo CE, Harding SM, Marcus C, Vaughn BV, et al. The AASM manual for the scoring of sleep and associated events. Rules, Terminology and Technical Specifications, Darien, Illinois, American Academy of Sleep Medicine 2012; 176:2012.
- [5] Fiorillo L, Puiatti A, Papandrea M, Ratti PL, Favaro P, Roth C, Bargiotas P, Bassetti CL, and Faraci FD. Automated sleep scoring: A review of the latest approaches. *Sleep medicine reviews* 2019; 48:101204 . doi: 10.1016/j.smr.2019.07.007.
- [6] Imtiaz SA. A systematic review of sensing technologies for wearable sleep staging. *Sensors* 2021; 21:1562. doi: 10.3390/s21051562.
- [7] Looney D, Kidmose P, Park C, Ungstrup M, Rank ML, Rosenkranz K, and Mandic DP. The in-the-ear recording concept: User-centered and wearable brain monitoring. *IEEE pulse* 2012; 3:32–42. doi: 10.1109/MPUL.2012.2216717.
- [8] Nakamura T, Goverdovsky V, Morrell MJ, and Mandic DP. Automatic sleep monitoring using ear-EEG. *IEEE journal of translational engineering in health and medicine* 2017; 5:1–8. doi: 10.1109/JTEHM.2017.2702558.
- [9] Mikkelsen KB, Villadsen DB, Otto M, and Kidmose P. Automatic sleep staging using ear-EEG. *Biomedical engineering online* 2017; 16:1–15. doi: 10.1186/s12938-017-0400-5.
- [10] Mikkelsen KB, Ebajemito JK, Bonmati-Carrion MA, Santhi N, Revell VL, Atzori G, Della Monica C, Debener S, Dijk DJ, Sterr A, et al. Machinelearning-derived sleep–wake staging from around-the-ear electroencephalogram outperforms manual scoring and actigraphy. *Journal of sleep research* 2019; 28:e12786. doi: 10.1111/jsr.12786.
- [11] Mikkelsen KB, Tabar YR, Kappel SL, Christensen CB, Toft HO, Hemmsen MC, Rank ML, Otto M, and Kidmose P. Accurate whole-night sleep monitoring with dry-contact ear-EEG. *Scientific reports* 2019; 9:16824. doi: 10.1038/s41598-019-53115-3.

- [12] Nakamura T, Alqurashi YD, Morrell MJ, and Mandic DP. Hearables: automatic overnight sleep monitoring with standardized in-ear-EEG sensor. *IEEE Transactions on Biomedical Engineering* 2019; 67:203–12. doi: 10.1109/TBME.2019.2911423.
- [13] Tabar YR, Mikkelsen KB, Rank ML, Hemmsen MC, Otto M, and Kidmose P. Ear-EEG for sleep assessment: a comparison with actigraphy and PSG. *Sleep and Breathing* 2021; 25:1693–705. doi: 10.1007/s11325-020-02248-1.
- [14] Jørgensen SD, Zibrandtsen IC, and Kjaer TW. Ear-EEG-based sleep scoring in epilepsy: A comparison with scalp-EEG. *Journal of Sleep Research* 2020; 29:e12921. doi: 10.1111/jsr.12921.
- [15] Kjaer TW, Rank ML, Hemmsen MC, Kidmose P, and Mikkelsen K. Repeated automatic sleep scoring based on ear-EEG is a valuable alternative to manually scored polysomnography. *PLOS Digital Health* 2022; 1:e0000134. doi: 10.1371/journal.pdig.0000134.
- [16] Silva Souto CF da, Pätzold W, Wolf KI, Paul M, Matthiesen I, Bleichner MG, and Debener S. Flex-printed ear-EEG sensors for adequate sleep staging at home. *Frontiers in Digital Health* 2021; 3:688122. doi: 10.3389/fdgth.2021.688122.
- [17] Buysse DJ, Reynolds III CF, Monk TH, Berman SR, and Kupfer DJ. The Pittsburgh Sleep Quality Index: a new instrument for psychiatric practice and research. *Psychiatry research* 1989; 28:193–213. doi: 10.1016/0165-1781(89)90047-4.
- [18] Åkerstedt T and Gillberg M. Subjective and objective sleepiness in the active individual. *International journal of neuroscience* 1990; 52:29–37. doi: 10.3109/00207459008994241.
- [19] Fiorillo L, Pedroncelli D, Agostini V, Favaro P, and Faraci FD. Multi-scored sleep databases: how to exploit the multiple-labels in automated sleep scoring. *Sleep* 2023; 46:zsad028. doi: 10.1093/sleep/zsad028.
- [20] Guillot A, Sauvet F, During EH, and Thorey V. Dreem open datasets: Multiscored sleep datasets to compare human and automated sleep staging. *IEEE transactions on neural systems and rehabilitation engineering* 2020; 28:1955– 65. doi: 10.1109/TNSRE.2020.3011181.

- [21] Lee YJ, Lee JY, Cho JH, and Choi JH. Interrater reliability of sleep stage scoring: a meta-analysis. *Journal of Clinical Sleep Medicine* 2022; 18:193–202. doi: 10.5664/jcsm.9538.
- [22] Delgado-Bonal A and Marshak A. Approximate entropy and sample entropy: A comprehensive tutorial. *Entropy* 2019; 21:541. doi: 10.3390/e21060541.
- [23] Min J, Wang P, and Hu J. Driver fatigue detection through multiple entropy fusion analysis in an EEG-based system. *PLoS one* 2017; 12:e0188756. doi: 10.1371/journal.pone.0188756.
- [24] Molina-Picó A, Cuesta-Frau D, Aboy M, Crespo C, Miró-Martínez P, and Oltra-Crespo S. Comparative study of approximate entropy and sample entropy robustness to spikes. *Artificial intelligence in medicine* 2011; 53:97– 106. doi: 10.1016/j.artmed.2011.06.007.
- [25] Wu J, Zhou T, and Li T. Detecting epileptic seizures in EEG signals with complementary ensemble empirical mode decomposition and extreme gradient boosting. *Entropy* 2020; 22:140. doi: 10.3390/e22020140.
- [26] Krishnan PT, Raj ANJ, Balasubramanian P, and Chen Y. Schizophrenia detection using Multivariate Empirical Mode Decomposition and entropy measures from multichannel EEG signal. *Biocybernetics and Biomedical Engineering* 2020; 40:1124–39. doi: 10.1016/j.bbe.2020.05.008.
- [27] Deng B, Cai L, Li S, Wang R, Yu H, Chen Y, and Wang J. Multivariate multi-scale weighted permutation entropy analysis of EEG complexity for Alzheimer's disease. *Cognitive neurodynamics* 2017; 11:217–31. doi: 10.1007/s11571-016-9418-9.
- [28] Aboy M, Hornero R, Abásolo D, and Álvarez D. Interpretation of the LempelZiv complexity measure in the context of biomedical signal analysis. *IEEE transactions on biomedical engineering* 2006; 53:2282–8. doi: 10.1109/TBME.2006.883696.
- [29] Lee JM, Kim DJ, Kim IY, Park KS, and Kim SI. Detrended fluctuation analysis of EEG in sleep apnea using MIT/BIH polysomnography data. *Computers in biology and medicine* 2002; 32:37–47. doi: 10.1016/s0010-4825(01)00031-2.

- [30] Vallat R and Walker MP. An open-source, high-performance tool for automated sleep staging. *Elife* 2021; 10:e70092. doi: 10.7554/eLife.70092.
- [31] Hjorth B. EEG analysis based on time domain properties. *Electroencephalography and clinical neurophysiology* 1970; 29:306–10. doi: 10.1016/0013-4694(70)90143-4.
- [32] Lal U, Mathavu Vasanthana S, and Hoblidar A. Temporal Feature Extraction and Machine Learning for Classification of Sleep Stages Using Telemetry Polysomnography. *Brain Sciences* 2023; 13:1201. doi: 10.3390/brainsci13081201.
- [33] Yan R, Zhang C, Spruyt K, Wei L, Wang Z, Tian L, Li X, Ristaniemi T, Zhang J, and Cong F. Multi-modality of polysomnography signals' fusion for automatic sleep scoring. *Biomedical Signal Processing and Control* 2019; 49:14–23. doi: 10.1016/j.bspc.2018.10.001.
- [34] Hadjidimitriou S, Zacharakis A, Doulgeris P, Panoulas K, Hadjileontiadis L, and Panas S. Sensorimotor cortical response during motion reflecting audiovisual stimulation: evidence from fractal EEG analysis. *Medical & biological engineering & computing* 2010; 48:561–72. doi: 10.1007/s11517-010-0606-1.
- [35] Asirvadam VS, Yusoff MZ, et al. Fractal dimension and power spectrum of electroencephalography signals of sleep inertia state. *IEEE Access* 2019; 7:185879–92. doi: 10.1109/ACCESS.2019.2960852.
- [36] Welch P. The use of fast Fourier transform for the estimation of power spectra: a method based on time averaging over short, modified periodograms. *IEEE Transactions on audio and electroacoustics* 1967; 15:70–3. doi: 10.1109/TAU.1967.1161901.
- [37] Geng D, Wang C, Fu Z, Zhang Y, Yang K, and An H. Sleep EEG-Based Approach to Detect Mild Cognitive Impairment. *Frontiers in Aging Neuroscience* 2022; 14:865558. doi: 10.3389/fnagi.2022.865558.
- [38] Huang D, Lin P, Fei DY, Chen X, and Bai O. Decoding human motor activity from EEG single trials for a discrete two-dimensional cursor control. *Journal of neural engineering* 2009; 6:046005. doi: 10.1088/1741-2560/6/4/046005.



- [39] Memar P and Faradji F. A novel multi-class EEG-based sleep stage classification system. *IEEE Transactions on Neural Systems and Rehabilitation Engineering* 2017; 26:84–95. doi: 10.1109/TNSRE.2017.2776149.
- [40] Mera-Gaona M, López DM, and Vargas-Canas R. An Ensemble feature selection approach to identify relevant features from EEG signals. *Applied Sciences* 2021; 11:6983. doi: 10.3390/app11156983.
- [41] Hassan AR, Bashar SK, and Bhuiyan MIH. Automatic classification of sleep stages from single-channel electroencephalogram. 2015 annual IEEE India conference (INDICON). IEEE. 2015 :1–6. doi: 10.1109/INDICON.2015.7443756.
- [42] Sharma N, Kolekar M, Jha K, and Kumar Y. EEG and cognitive biomarkers based mild cognitive impairment diagnosis. *Irbm* 2019; 40:113–21. doi: 10.1016/j.irbm.2018.11.007.
- [43] Choudhury AR, Ghosh A, Pandey R, and Barman S. Emotion recognition from speech signals using excitation source and spectral features. 2018 IEEE Applied Signal Processing Conference (ASPCON). IEEE. 2018 :257–61. doi: 10.1109/ASPCON.2018.8748626.
- [44] Mitra P, Murthy C, and Pal SK. Unsupervised feature selection using feature similarity. *IEEE transactions on pattern analysis and machine intelligence* 2002; 24:301–12. doi: 10.1109/34.990133.
- [45] Solorio-Fernández S, Carrasco-Ochoa JA, and Martínez-Trinidad JF. A review of unsupervised feature selection methods. *Artificial Intelligence Review* 2020; 53:907–48. doi: 10.1007/s10462-019-09682-y.
- [46] Yan X, Nazmi S, Erol BA, Homaifar A, Gebru B, and Tunstel E. An efficient unsupervised feature selection procedure through feature clustering. *Pattern Recognition Letters* 2020; 131:277–84. doi: 10.1016/j.patrec.2019.12.022.
- [47] Zhao Z, Wang L, Liu H, and Ye J. On similarity preserving feature selection. *IEEE Transactions on Knowledge and Data Engineering* 2011; 25:619–32. doi: 10.1109/TKDE.2011.222.

- [48] Klumpe H, Lugagne JB, Khalil AS, and Dunlop M. Deep neural networks for predicting single cell responses and probability landscapes. *bioRxiv* 2023 :2023–6. doi: 10.1021/acssynbio.3c00203.
- [49] Dragalin V, Fedorov V, Patterson S, and Jones B. Kullback–Leibler divergence for evaluating bioequivalence. *Statistics in medicine* 2003; 22:913–30. doi: 10.1002/sim.1451.
- [50] Bullmann M, Fetzner T, Ebner F, Deinzer F, and Grzegorzec M. Fast kernel density estimation using Gaussian filter approximation. 2018 21st International Conference on Information Fusion (FUSION). IEEE. 2018 :1233–40. doi: 10.23919/ICIF.2018.8455686.

## Tables

**Table 1**

Number and percentage of 30-second epochs per sleep stage (i.e., the result of the consensus reached by the three different scorers) for both PSG and in-ear-EEG based scoring procedure, and the intersection ( $\cap$ ) computed on the labels coming from the two different sources.

	<i>W</i>	<i>NREM</i>	<i>REM</i>	<i>Total</i>
<b>PSG</b>	344 (7.5%)	3469 (75.9%)	755 (16.5%)	4568
<b>In-ear-EEG</b>	277 (6.1%)	3768 (82.5%)	523 (11.4%)	4568
<b>PSG <math>\cap</math> In-ear-EEG</b>	236 (6.0%)	3308 (84.0%)	392 (10.0%)	3936

# Figures

**Figure 1.** Schematic layout of the clinical study and the data collection procedure.

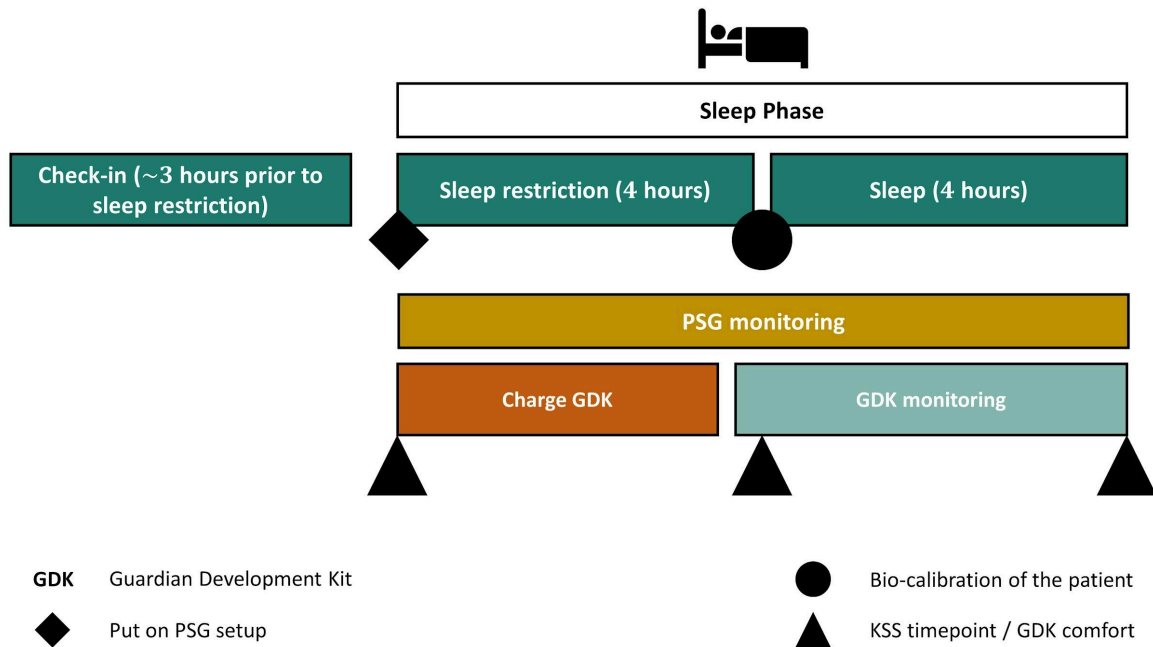


**Figure 2.** Devices employed in the data collection: a) SOMNOmedics SOMNOscreen plus system for PSG data with the EXG configuration, i.e., including six scalp electrodes, EOG and ECG signal monitoring; b) Guardian Development Kit (GDK) hardware including ear tips, earpieces, and brain box used to record in-ear-EEG data.

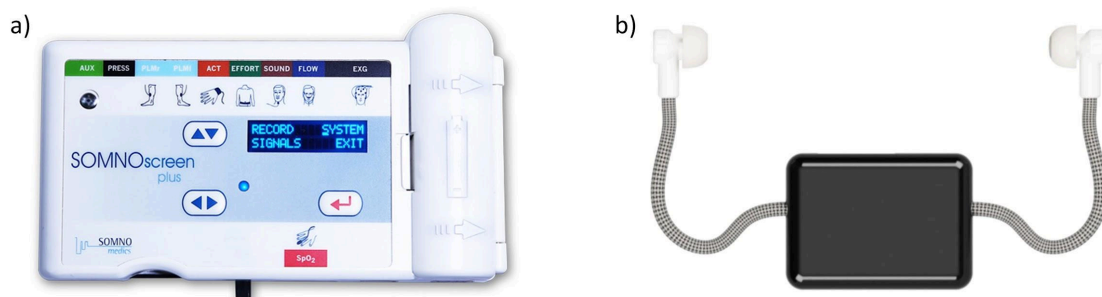


**Figure 3.** Workflow for evaluating the similarity between the signals recorded from two different channels, including feature extraction and feature selection, separately for each sleep stage; and the comparison between feature distributions using the Jensen–Shannon divergence before the assessment of the similarity-scores, individually for each sleep stage and for each subject. In detail, a) refers to the comparison between one in-ear-EEG and one PSG channel (either scalp-EEG or EOG channels); while b) illustrates the analysis between two PSG channels (either scalp-EEG or EOG channels). An example of similarity-scores distribution for awake, NREM and REM classes is included for both cases study.

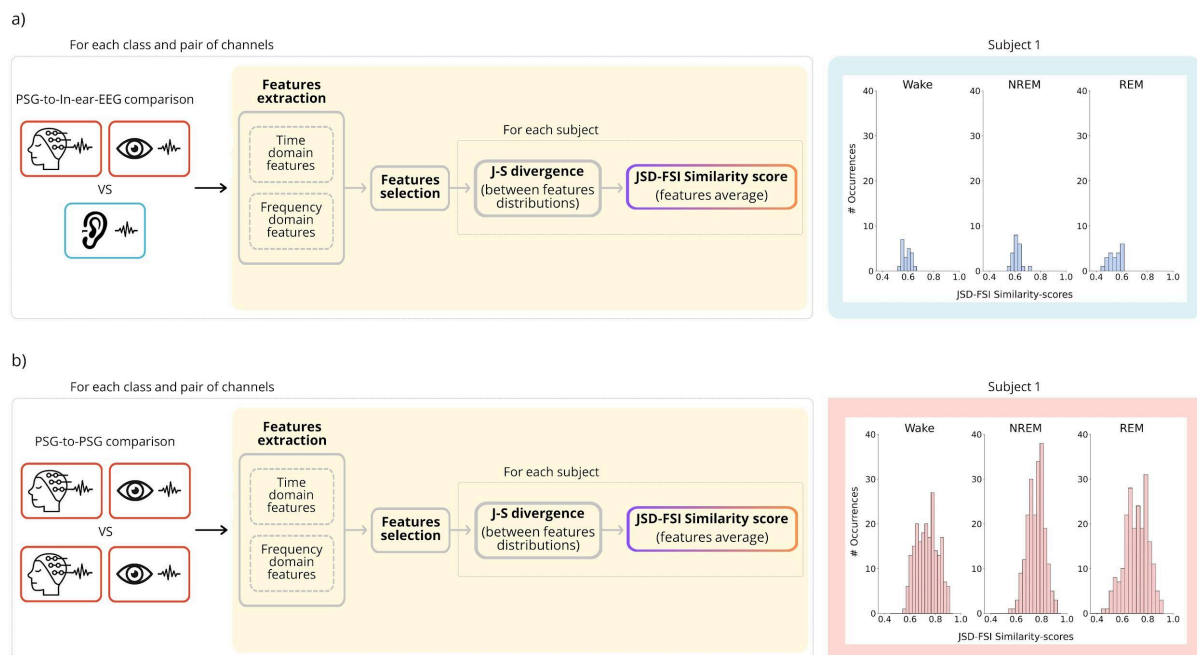


**Figure 4.** Intra-scorer variability (multi-source-scored dataset). Boxplot distribution of the Cohen's kappa values computed for each recording/subject between the PSG and in-ear-EEG hypnograms - for each scorer.

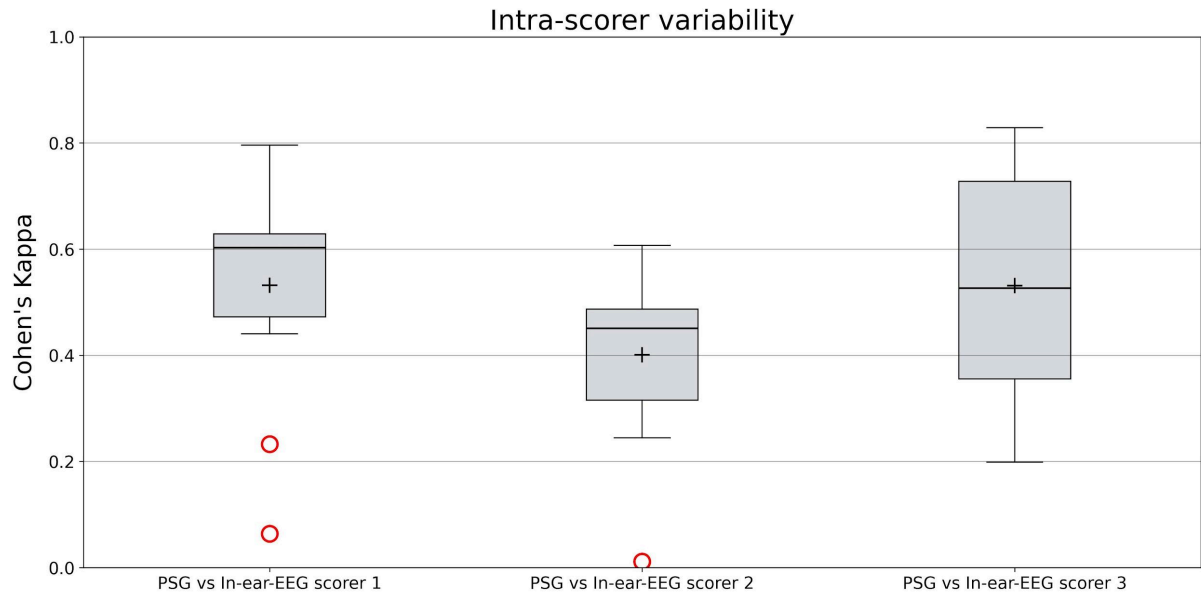


**Figure 5.** Inter-scorer variability (multi-source-scored dataset). Boxplot distributions of the Cohen's kappa values computed for each recording/subject between the three scorer experts for in-ear-EEG (in red) and PSG (in blue) signals.

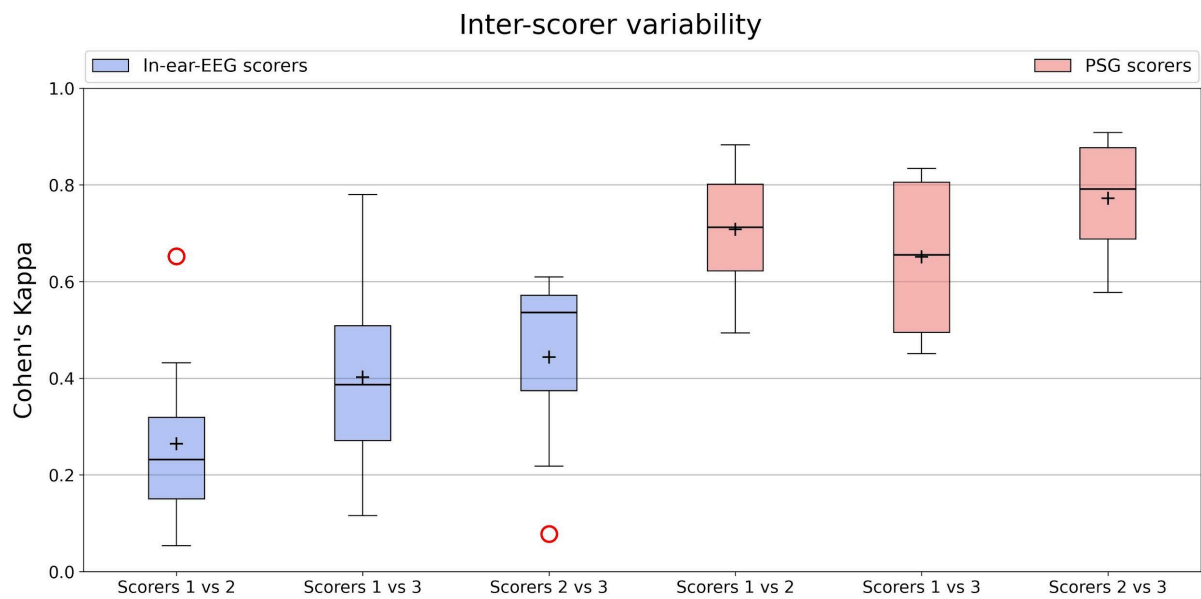


**Figure 6.** Color-coded heatmap showing the selection frequency of each extracted feature across the various subsets  $\{D^q, D^{CH1}\}$ , separately for each sleep stage, reporting warmer colors for higher frequencies.

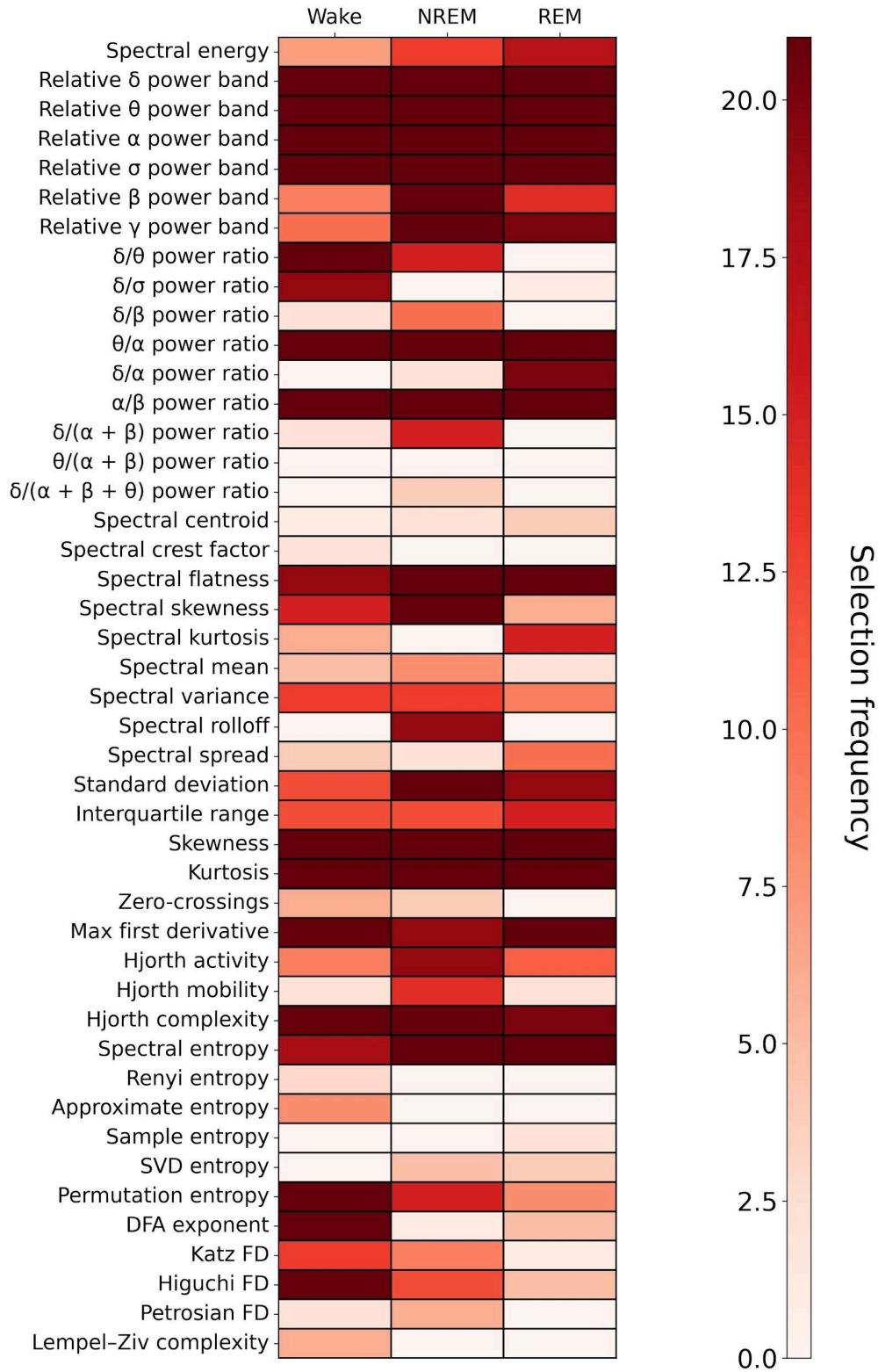


**Figure 7.** Head topography plots of JSD-FSI similarity-scores of the in-ear-EEG with respect to the PSG channels in the  $Q$  set (EEG and EOG channels) - for each subject in the awake stage. Unipolar channels represented as markers; bipolar channels represented as lines. The mean and the standard deviation of the similarity-scores distribution computed for each subject is also included.

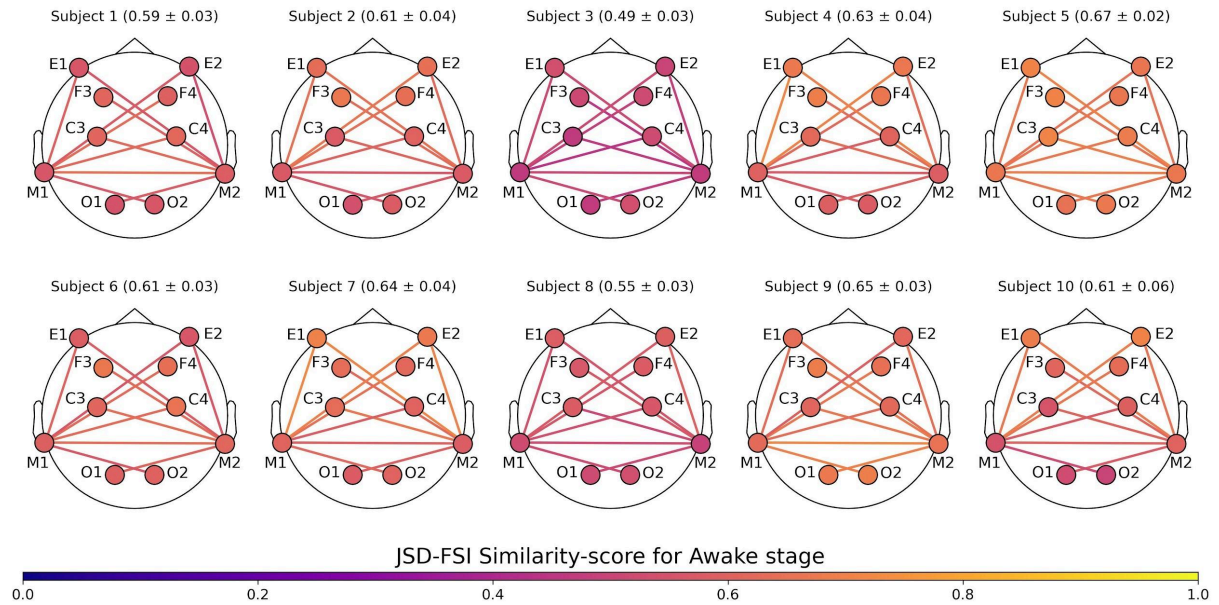




**Figure 8.** Head topography plots of JSD-FSI similarity-scores of the in-ear-EEG with respect to the PSG channels in the  $Q$  set (EEG and EOG channels) - for each subject in the awake stage. Unipolar channels represented as markers; bipolar channels represented as lines. The mean and the standard deviation of the similarity-scores distribution computed for each subject is also included.

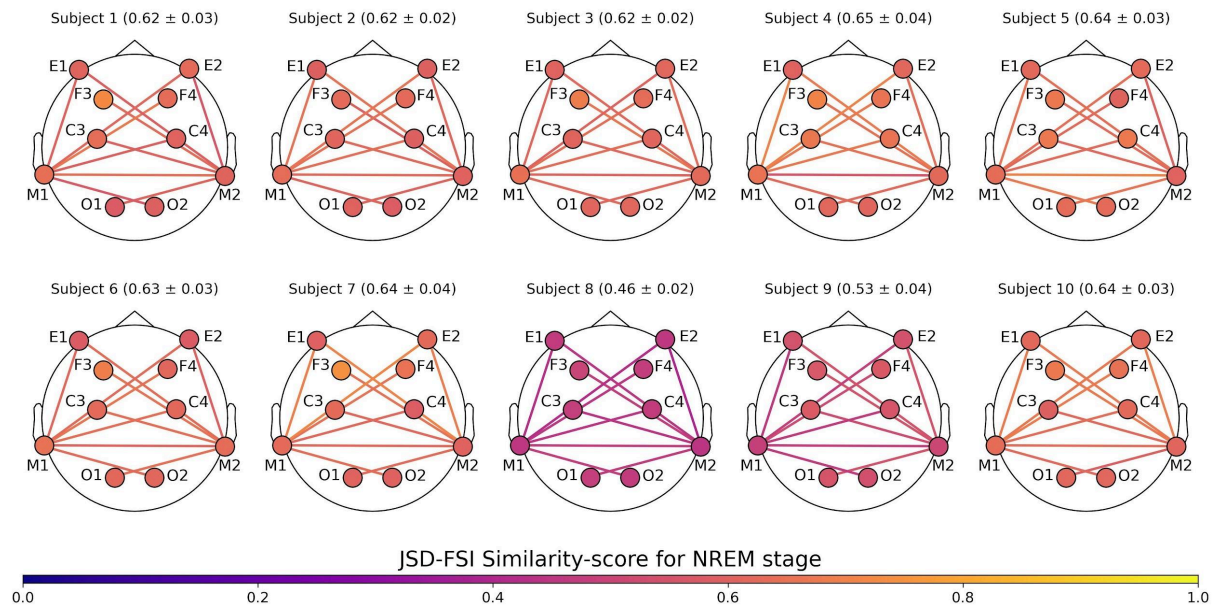


**Figure 9.** Head topography plots of JSD-FSI similarity-scores of the in-ear-EEG with respect to the PSG channels in the  $Q$  set (EEG and EOG channels) - for each subject in the REM sleep stage. Unipolar channels represented as markers; bipolar channels represented as lines. The mean and the standard deviation of the similarity-scores distribution computed for each subject is also included. No JSD-FSI similarity-scores reported for subjects 3 and 8 due to the lack of REM epochs following PSG and in-ear-EEG consensus intersection.

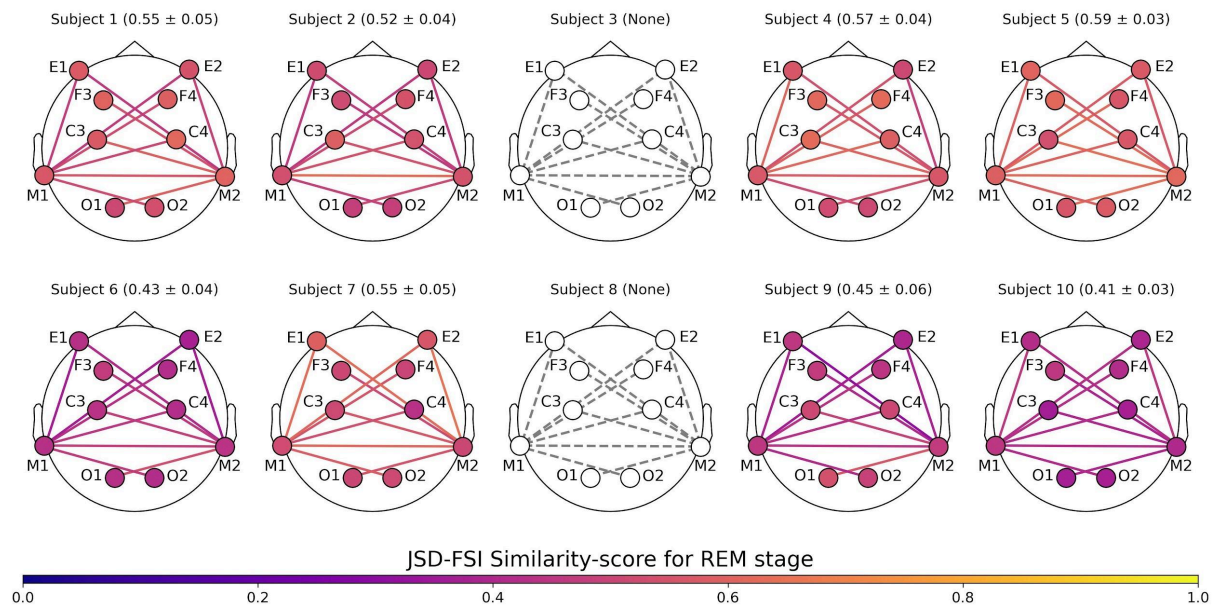


**Figure 10.** JSD-FSI similarity-scores distributions, i.e., distributions derived from the PSG-to-In-ear (histograms in blue) and PSG-to-PSG (histograms in red) comparisons - for each subject in the awake stage.

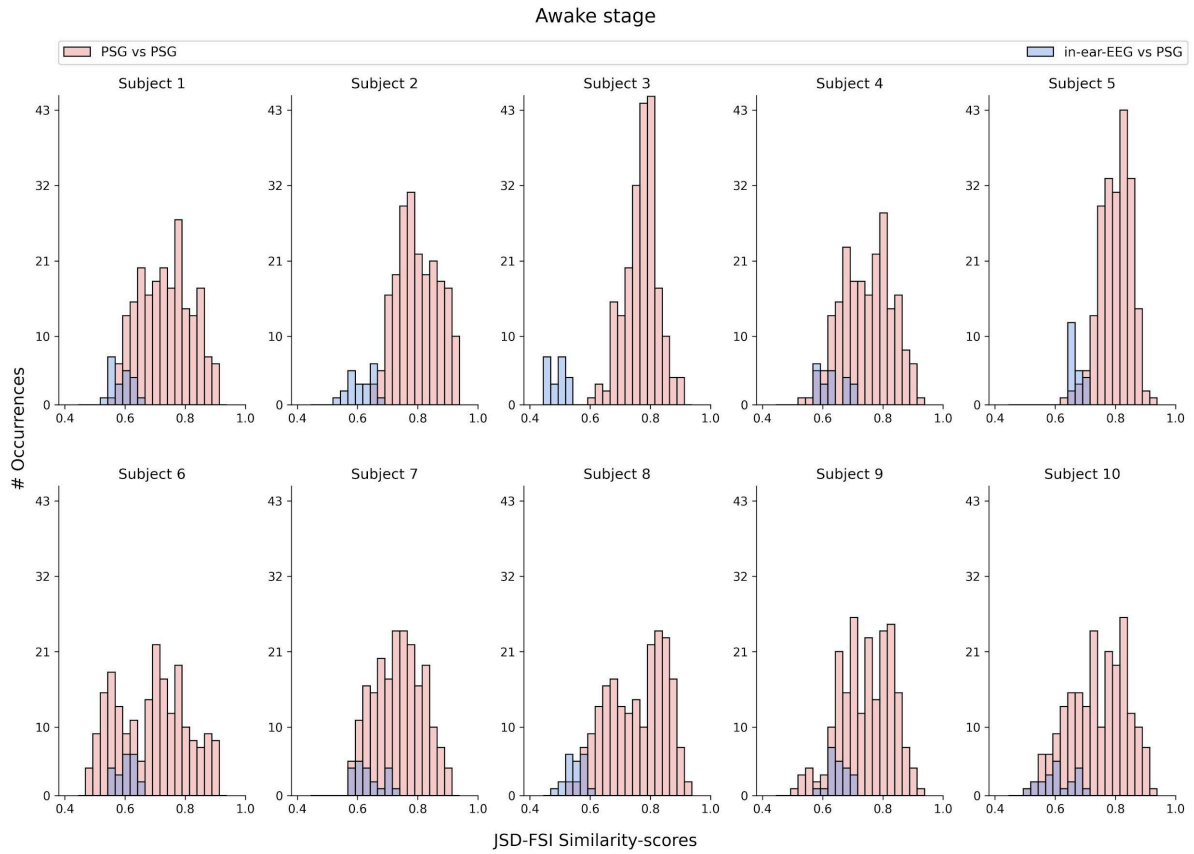


**Figure 11.** JSD-FSI similarity-scores distributions, i.e., distributions derived from the PSG-to-In-ear (histograms in blue) and PSG-to-PSG (histograms in red) comparisons - for each subject in the NREM sleep stage.

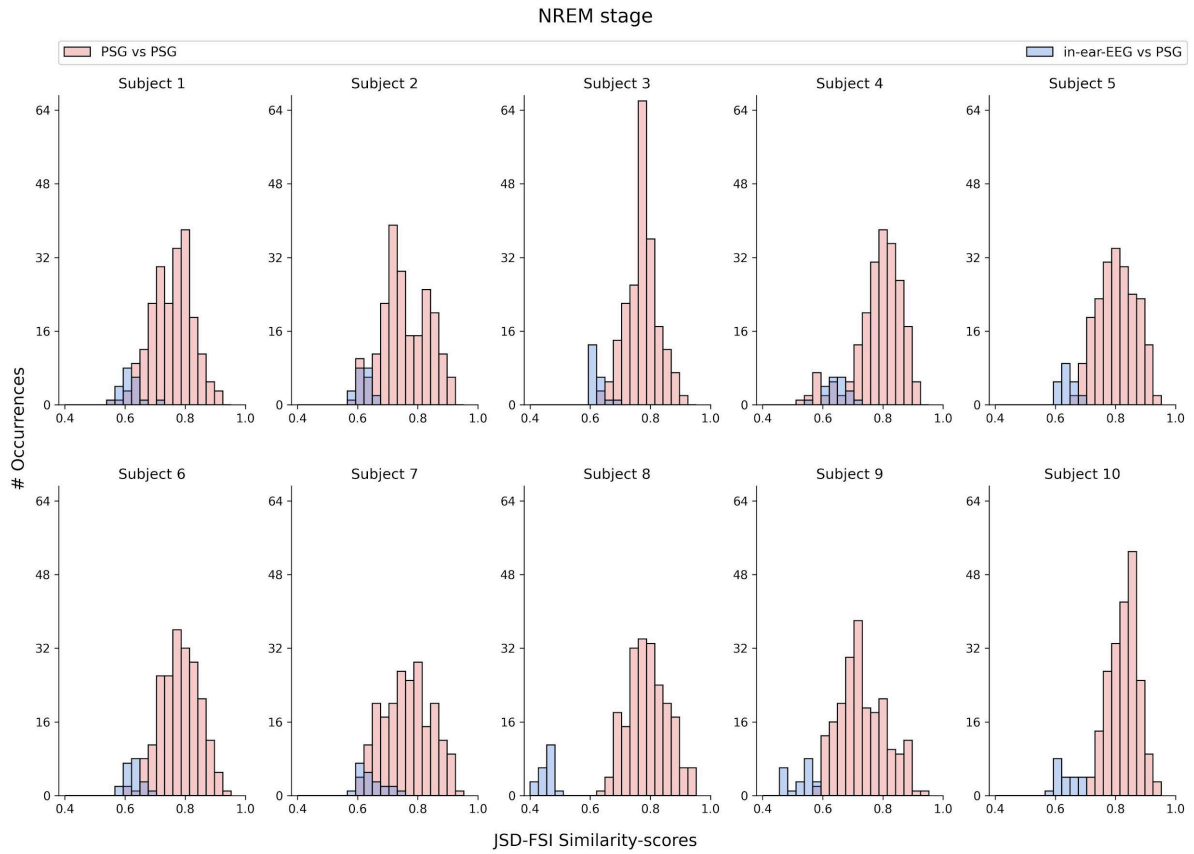
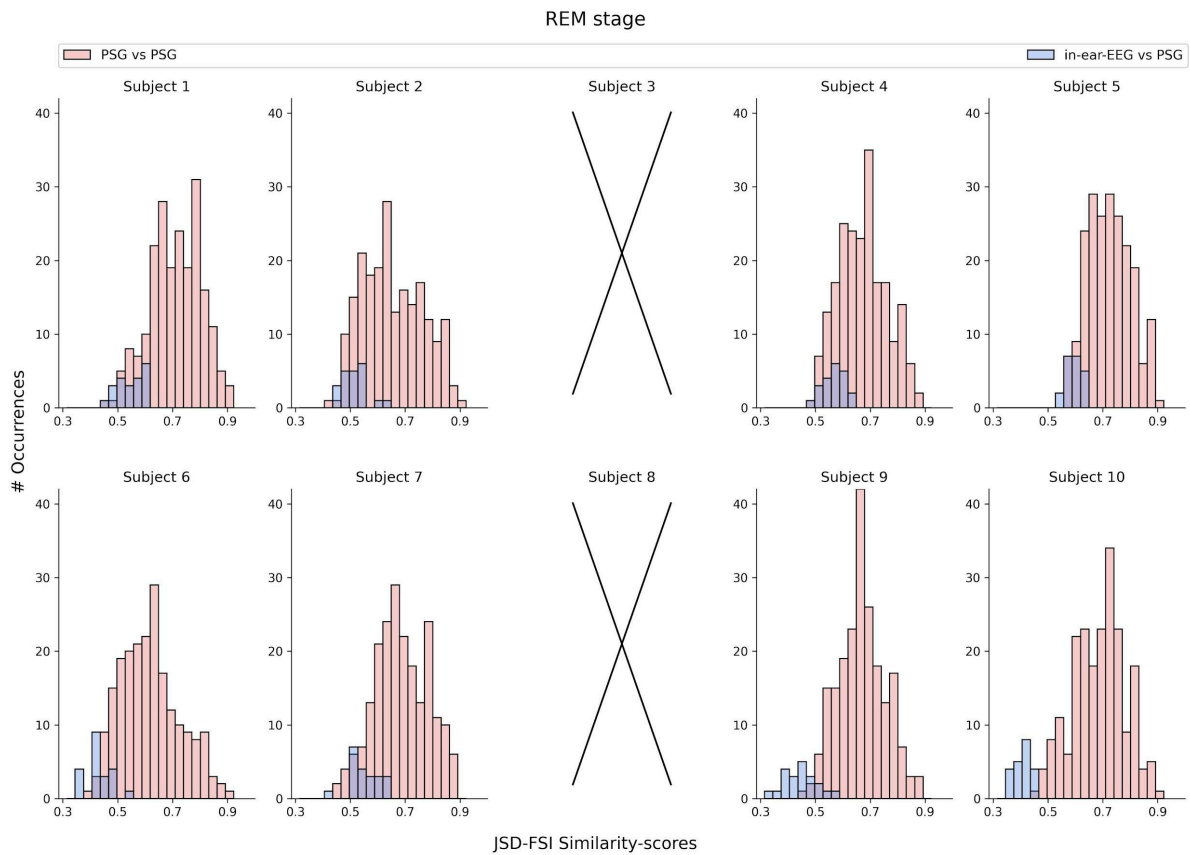


**Figure 12.** JSD-FSI similarity-scores distributions, i.e., distributions derived from the PSG-to-In-ear (histograms in blue) and PSG-to-PSG (histograms in red) comparisons - for each subject in the REM sleep stage. No JSD-FSI similarity-scores reported for subjects 3 and 8 due to the lack of REM epochs following PSG and in-ear-EEG consensus intersection.



# **SUPPLEMENTARY MATERIAL**

## **Comparison analysis between standard polysomnographic data and in-ear-EEG signals: A preliminary study**

Gianpaolo Palo<sup>1,2,†</sup>, Luigi Fiorillo<sup>1,\* †</sup>, Giuliana Monachino<sup>1,3</sup>, Michal Bechny<sup>1,3</sup>, Mark Melnykowycz<sup>4</sup>, Athina Tzovara<sup>3</sup>, Valentina Agostini<sup>2</sup>, and Francesca Dalia Faraci<sup>1</sup>

<sup>1</sup>Institute of Digital Technologies for Personalized Healthcare (MeDiTech), Department of Innovative Technologies, University of Applied Sciences and Arts of Southern Switzerland, Lugano, Switzerland; <sup>2</sup>Department of Electronics and Telecommunications, Politecnico di Torino, Torino, Italy; <sup>3</sup>Institute of Computer Science, University of Bern, Bern, Switzerland; <sup>4</sup>IDUN Technologies AG, Glattpark, Switzerland.

Institution where work was performed: Institute of Digital Technologies for Personalized Healthcare (MeDiTech), Department of Innovative Technologies, University of Applied Sciences and Arts of Southern Switzerland, Lugano, Switzerland.

†These authors contributed equally to this work.

\*Corresponding author - Email: [luigi.fiorillo@supsi.ch](mailto:luigi.fiorillo@supsi.ch).

# SUPPLEMENTARY ANALYSES

## Time-domain features

In the list below we report mathematical details on how to compute each feature.

- **Standard deviation** and **interquartile range (IQR)** are statistical measures of dispersion, and are exploited in our study to describe the variation of the electrical activity in the brain.
- **Skewness** and **kurtosis** are the third and fourth central moment in statistics, and are used to characterize the shape of the EEG signals in terms of asymmetry relative to the mean and heaviness of the tails compared to a normal distribution.
- The **maximum first derivative** and the **number of zero-crossings** give information about the depolarization of an EEG recording. The former outlines the highest rate of depolarization in the signal, while the latter estimates its frequency of sign-changes.
- **Approximate entropy** and **sample entropy** are two time series regularity metrics. In general, entropy measures evaluate the complexity of a time series by estimating its intrinsic disorder. The higher the entropy of a signal, the less predictable its evolution. The approximate entropy,  $ApEn(1)$ , quantifies the logarithmic likelihood that a signal of length  $N$  repeats itself always the same within a certain tolerance  $r$ . Its estimation includes dividing the signal in sub-segments first of length  $d$  and then  $(d + 1)$  before evaluating the correlation integral,  $C(r)$ , which expresses how many times each  $i$ -th sub-segment is akin to all the others [22, 24].

$$ApEn(d, r, N) = \frac{\sum_{i=1}^{N-d+1} \log[C_i^d(r)]}{N-d+1} - \frac{\sum_{i=1}^{N-(d+1)+1} \log[C_i^{d+1}(r)]}{N-(d+1)+1} \quad (1)$$

The sample entropy,  $SpEn$  (2), can be taken as a simpler version of the approximate entropy. The difference lies in no longer considering the self-matching for each sub-segment [22].

$$SpEn(d, r, N) = -\frac{1}{N-d+1} \log \left[ \frac{\sum_{i=1}^{N-d+1} C_i^{d+1}(r)}{\sum_{i=1}^{N-d+1} C_i^d(r)} \right] \quad (2)$$

Parameters  $d$  and  $r$  are respectively set to 2 and  $0.2 \cdot SD$  ( $SD$ : standard deviation of the signal) for both  $ApEn$  and  $SpEn$  [23-25].

- **Singular Value Decomposition entropy (SVDEn)**, quantifies the complexity of the time series based on the number of eigenvectors needed for its adequate representation. Mathematically, starting from a signal of length  $N$ , i.e.,  $[x_1, x_2, \dots, x_N]$  some delay vectors  $y(i) = [x_i, x_{i+\tau}, \dots, x_{i+(d_E-1)\tau}]$  are built, having  $i = 1, 2, \dots, N$ . Two parameters are involved, i.e., the embedded dimension ( $d_E$ ) and the delay ( $\tau$ ), which are respectively set to 3 and 1, as recommended for short duration EEG signals [25, 26]. SVD factorization is then performed on the embedded matrix  $Y = [y(1), y(2), \dots, y(N - (d_E - 1)\tau)]$ , resulting in  $M$  singular values  $(\sigma_1, \sigma_2, \dots, \sigma_M)$ .

Hence, SVD entropy is computed on normalized singular values, such that

$$\bar{\sigma}_i = \sigma_i / \sum_{j=1}^M \sigma_j, \text{ following (3) [26].}$$



$$SVDEn = - \sum_{i=1}^M \overline{\sigma}_i \log_2(\overline{\sigma}_i) \quad (3)$$

- **Permutation entropy (PermEn)**, involves the partition of the time series of length  $N$  into a matrix of overlapping column vectors of length  $D$ . The overlap is defined by a delay parameter ( $\tau$ ). In this work,  $D = 3$  and  $\tau = 1$  [25, 27]. Column vectors are then mapped into permutations ( $\pi$ ) capturing the ordinal rankings of data. Hence, permutation entropy is calculated as shown in (4), where  $p_i$  is the relative frequency of the  $i$ -th permutation ( $\pi_i$ ) and is evaluated as the number of times  $\pi_i$  is found in the signal over the total number of sequences [25, 27].

$$SVDEn = - \sum_{i=1}^{D!} p_i \log_2(p_i) \quad (4)$$

- **Lempel-Ziv complexity (C)**, evaluates the randomness of the time series. First, the signal of length  $N$  is transformed into a binary sequence using coarse-graining. This is performed by assigning 0 and 1 to values respectively below and above a threshold. The latter is defined as the median of the window time series analyzed for its robustness to possible outliers [28]. While inspecting the signal from left to right, the overall number of distinct subsequences,  $c(N)$ , of consecutive characters is assessed. To get a measure that is independent of the sequence length, Lempel-Ziv complexity is defined as the normalized version of  $c(N)$  (5).

$$C(N) = c(N) \frac{\log_2(N)}{N} \quad (5)$$

- **Detrended Fluctuation Analysis (DFA)** exponent,  $\alpha$ , measures the degree of long-term statistical dependencies or intrinsic self-similarity in time series. This

feature is used to quantify the long-range correlation properties of the EEG signal by evaluating possible self-similar patterns in the electrical activity of the brain. First, the time series  $x$  of length  $N$  is integrated to define the '*accumulated walk*',  $y(k)$  (6).

$$y(k) = \sum_{i=1}^k [x(i) - \bar{x}] \quad (6)$$

where  $x(i)$  is the sequence at the  $i$ -th sample, and  $\bar{x}$  is the mean of the entire time series. Hence,  $y(k)$  is divided into sub-sequences of equal length  $n$ , and a least-squares line fitting the data within each sub-sequence is evaluated. The y-coordinate of the latter,  $y_n(i)$ , describes the local trend of each sub-sequence. The Root-Mean-Square (RMS) fluctuation,  $F(n)$  (7), is then calculated by integrating and detrending  $y(k)$ .

$$F(n) = \sqrt{\frac{1}{N} \sum_{i=1}^N [y(i) - y_n(i)]^2} \quad (7)$$

The whole process is iterated over all the possible lengths,  $n$ . The DFA exponent is defined as the slope of the best-fitting line to the distribution of the RMS fluctuation as a function of the segment size on a log-log scale.

Whether  $\alpha > 0.5$ , the time series is characterized by long-range correlations, while  $\alpha < 0.5$  outlines that the signal is *antipersistent*, i.e., it shows a negative correlation. The case  $\alpha = 0.5$  indicates that changes in time series are random and uncorrelated with each other, thus the signal can be modeled as *white noise* [29, 30].

- **Hjorth parameters**, i.e., **activity**  $H_A$ , **mobility**  $H_M$ , and **complexity**  $H_C$ , are statistical functions based on first and second derivatives of time series useful to characterize the dynamics of the brain function. Let  $x$  be an EEG signal of length  $N$  and  $\bar{x}$  be its mean value,  $H_A$  (8) provides information about its energy;  $H_M$  (8) is introduced to assess the variability of its frequency over time; and  $H_C$  (8) gives insights into the

complexity of its waveform in terms of amplitude and frequency with respect to a common sine wave [31].

$$H_A = var[x(t)] = \frac{\sum_{i=1}^N (x_i - \bar{x})^2}{N}; \quad H_M = \sqrt{\frac{var\left[\frac{d}{dt}x(t)\right]}{H_A}}; \quad H_C = \frac{H_M\left[\frac{d}{dt}x(t)\right]}{H_M[x(t)]} \quad (8)$$

- **Katz, Higuchi, and Petrosian** fractal dimensions estimate the fractality of the time series by measuring its complexity and self-similarity over different scales of observation [34].

According to Katz fractal dimension,  $FD_K$ , the complexity is defined based on the deviation of the trajectory of the time series from the simplest path, i.e., the straight line between the first and last points (9).

$$FD_K = \frac{\log(n)}{\log(n) + \log\left(\frac{d}{L}\right)} \quad (9)$$

where  $d$  is the farthest distance among all those measured between the first point of the signal and all the others;  $L$  is the total length of the waveform and is calculated as the sum of the distances between successive points of the signal; and  $n = L/a$  is the number of units that compose the time series. In particular, to avoid that different units lead to different fractal dimensions, a general unit,  $a$ , is defined as the average distance between subsequent points [34, 35].

Using Higuchi fractal dimension,  $FD_H$ , the complexity is assessed by analyzing how the pattern of the signal changes when sampled at different time intervals. First, starting from the time series  $x = x(1), x(2), \dots, x(N)$  of length  $N$ ,  $k$  new sequences are defined following (10), where  $m = 1, 2, \dots, k$  is the initial time value;  $k \in [1, k_{max}]$

is the discrete time delay; and  $[a]$  indicates the integer part of  $a$ . In this study,  $k = 10$  [32, 35].

$$x_k^m = \left[ x(m), x(m+k), x(m+2k), \dots, x\left(m + \lfloor \frac{N-m}{k} \rfloor k\right) \right] \quad (10)$$

The length of each  $x_k^m$  is evaluated,  $L_m(k)$  (11), before averaging all those associated with the same delay,  $k$  (12). Therefore,  $FD_H$  is determined as the slope of the least squares linear best fit to the distribution of  $L(k)$  versus  $1/k$  on a double logarithmic scale.

$$L_m(k) = \frac{N-1}{k} \left[ \frac{1}{\lfloor \frac{N-m}{k} \rfloor} \sum_{i=1}^{\lfloor (N-m)/k \rfloor} |x(m+ik) - x(m+(i-1)k)| \right] \frac{1}{k} \quad (11)$$

$$L(k) = \sum_{m=1}^k L_m(k) \propto k^{-FD_H} \quad (12)$$

Similarly to  $FD_K$ , Petrosian fractal dimension,  $FD_P$ , quantifies the complexity of the time series in relation to how much it deviates from a straight line. In particular, given a signal of length  $N$ , Petrosian's definition (13) focuses on the number of sign-changes in its first derivative, thus emphasizing the rate of slope reversals [33, 34].

$$FD_P = \frac{\log(N)}{\log(N) + \log\left(\frac{N}{N + 0.4N_\Delta}\right)} \quad (13)$$

## Frequency-domain features

In the list below we report mathematical details on how to compute each feature.

- **Spectral energy** represents the total energy of the time series and is defined by integrating the Power Spectral Density (PSD) of the signal.

**Relative powers** of all the EEG frequency bands, i.e., **delta** ( $\delta$ , 0.5–4 Hz), **theta** ( $\theta$ , 4–8 Hz), **alpha** ( $\alpha$ , 8–12 Hz), **sigma** ( $\sigma$ , 12–16 Hz), **beta** ( $\beta$ , 16–30 Hz), and **gamma** ( $\gamma$ , 30–35 Hz) are also calculated. These estimate how the signal energy is distributed across its several frequency components.

In addition, several **ratios between frequency bands** are included as features, i.e.,  $\delta/\theta$ ,  $\delta/\sigma$ ,  $\delta/\beta$ ,  $\theta/\alpha$ ,  $\delta/\alpha$ ,  $\alpha/\beta$ ,  $\delta/(\alpha + \beta)$ ,  $\theta/(\alpha + \beta)$ ,  $\delta/(\alpha + \beta + \theta)$ .

- Unlike previous entropy metrics, **spectral entropy**, **SpecEn** (14), and **Renyi entropy**, **RenyiEn** (15) are measured in the frequency domain. In particular, they assess the complexity of the EEG signal by working on its normalized power spectrum [39].

$$SpecEn = - \sum_f p(f) \log[p(f)] \quad (14)$$

$$RenyiEn = - \log \left[ \sum_f p^2(f) \right] \quad (15)$$

- **Spectral centroid** represents the center of mass of the spectrum of the time series and is calculated as the frequency-weighted mean of the PSD of the signal [40, 41].

- **Spectral flatness** is computed as the ratio of the geometric mean of the power spectrum to its arithmetic mean [40]. It evaluates how much noise-like the signal is [41].
- **Spectral spread** quantifies the dispersion of the power spectrum around its spectral centroid. Numerically, it is given by the weighted mean of the PSD of the signal and the weights are defined as the squared differences between the spectral centroid and all the examined frequencies [41].
- **Spectral crest factor** provides information about how extreme the peaks of the spectrum of the signal are. It is evaluated as the ratio of the maximum power spectrum to the mean PSD of the signal [42].
- **Spectral roll-off** is defined as the frequency beneath which a certain percentage of the overall energy lies. In this study, this feature is determined relative to 85% of the energy [43].
- The four **spectral central moments** in statistics, i.e., **mean**, **variance**, **skewness**, and **kurtosis**, provide insights into the shape and distribution of the PSD of the signal.

## Feature selection

The feature selection algorithm we choose relies on pairwise feature similarity, which is evaluated using the maximal information compression index (MICI). This metric has been shown to outperform two other commonly-used feature similarity measures [44, 46].

Let  $\Sigma$  be the two-by-two covariance matrix of features  $x$  and  $y$ ,  $\lambda_2$  is defined as the smallest eigenvalue of  $\Sigma$  (16, 17).

$$\lambda_2(x, y) = \frac{1}{2}[\text{var}(x) + \text{var}(y) - \sqrt{A(x, y)}] \quad (16)$$

$$A(x, y) = [\text{var}(x) + \text{var}(y)]^2 - 4\text{var}(x)\text{var}(y)[1 - \rho(x, y)^2] \quad (17)$$

where  $\text{var}$  stands for variance and  $\rho$  represents the Pearson's correlation coefficient.

In particular, what is used here is a modified version of the MICI, as it gets normalized by the sum of the variances of the features to not have sensitivity to the features' scale (18) [46].

$$\lambda_{2, \text{norm}}(x, y) = \frac{\lambda_2(x, y)}{\text{var}(x) + \text{var}(y)} \quad (18)$$

The Feature Selection using Feature Similarity (FSFS) algorithm [44] is based on the k-nearest neighbors (kNN) principle, i.e., it divides the initial feature subset into homogeneous clusters, before selecting only the most representative feature from each such cluster. Iteratively, the algorithm selects only the feature showing the most compact subset, i.e., the lowest distance from its farthest neighbor, thus removing all the k-nearest ones. A constant error threshold,  $\varepsilon$ , is defined by the MICI value between the feature selected at the first iteration and its k-th neighbor. This is used to adapt the algorithm in such a way that at each iteration whenever the smallest  $\lambda_2$  is lower than  $\varepsilon$ , the number of k-nearest neighbors (k) decreases [44].

The best initial value for k is set according to two metrics, i.e., the representation entropy ( $H_R$ ) (19) and the redundancy rate (RR) (20). The former quantifies the information compression. Higher values are linked to a more balanced feature selection process, i.e., lower redundancy within the feature subset [44, 45].

$$H_R = - \sum_{i=1}^N \hat{\lambda}_i \log \hat{\lambda}_i \quad (19)$$

where  $\hat{\lambda}_i$  is the normalized eigenvalue of the covariance matrix of the feature subset of size

$N$ , having  $i=1, 2, \dots, N$  and  $\hat{\lambda}_i = \lambda_i / \sum_{i=1}^N \lambda_i$ .

The redundancy rate evaluates the redundant information within the feature subset with larger values indicating a strong correlation among features [45, 47].

$$RR = \frac{1}{N(N-1)} \sum_{f_i, f_j \in F, i > j} \rho_{ij} \quad (20)$$

where  $\rho$  is the Pearson's correlation coefficient measured for each pair of features ( $f$ ) of the target subset ( $F$ ) of size  $N$ . The best number of  $k$ -nearest neighbors is independently found for each sleep stage and for each pair of PSG and in-ear-EEG channels as the one that maximizes  $H_R$ . Hence, the chosen  $k$ -value is validated by comparing the RR metrics between the reduced feature subset and the initial one.



## SUPPLEMENTARY TABLES

**Table S1.**

*Soft-Agreement* values computed on each of three scorers and for each subject on the PSG data source. For each subject, we report the most reliable scorer with the corresponding cell with edges highlighted in bold.

Soft-agreement for PSG scorers			
	Scorer 1	Scorer 2	Scorer 3
Subject 1	0.9133	0.8206	0.9456
Subject 2	0.8644	0.8745	0.8927
Subject 3	<b>0.8958</b>	0.8477	0.8417
Subject 4	0.8529	0.9125	0.9403
Subject 5	0.7819	0.9177	0.9197
Subject 6	<b>0.8206</b>	0.7794	0.8124
Subject 7	0.8809	0.7773	0.9258
Subject 8	0.7617	0.8398	0.8984
Subject 9	0.9238	0.8397	0.9399
Subject 10	0.8053	0.7930	0.9242
Averaged	0.8501 ± 0.0529	0.8402 ± 0.0477	<b>0.9041 ± 0.0423</b>

**Table S2.**

*Soft-Agreement* values computed on each of three scorers and for each subject on the in-ear-EEG data source. For each subject, we report the most reliable scorer with the corresponding cell with edges highlighted in bold.

Soft-agreement for in-ear-EEG scorers			
	Scorer 1	Scorer 2	Scorer 3
Subject 1	0.8226	<b>0.8548</b>	0.8125
Subject 2	0.7632	0.8219	<b>0.8381</b>
Subject 3	0.5030	0.6653	<b>0.6834</b>
Subject 4	0.6879	0.7714	<b>0.8489</b>
Subject 5	0.6975	0.8498	<b>0.8683</b>
Subject 6	0.6227	0.6742	<b>0.8887</b>
Subject 7	<b>0.8887</b>	0.7402	0.8555
Subject 8	0.5937	0.6484	<b>0.4297</b>
Subject 9	0.7194	<b>0.8637</b>	0.8617
Subject 10	0.6250	0.8402	<b>0.8033</b>
Averaged	0.6924 ± 0.1078	0.7730 ± 0.0810	0.7890 ± 0.1315

**Table S3.**

List of all the extracted time-domain features. Abbreviations: Detrended Fluctuation Analysis (DFA); Singular Value Decomposition (SVD). \* features depending on amplitude, thus computed on normalized signals.

<b>Time-domain features</b>		
Standard deviation*	DFA exponent	Hjorth activity*
Skewness	Approximate entropy	Hjorth mobility
Kurtosis	Sample entropy	Hjorth complexity
Maximum first derivative*	SVD entropy	Katz fractal dimension
Interquartile range*	Permutation entropy	Higuchi fractal dimension
Number of zero-crossings	Lempel-Ziv complexity	Petrosian fractal dimension

**Table S4.**

List of all the extracted frequency-domain features. \* features depending on amplitude, thus computed on normalized signals.

<b>Frequency-domain features</b>		
Spectral energy*	$\delta/\theta$ power ratio	Spectral centroid
Relative $\delta$ power band	$\delta/\sigma$ power ratio	Spectral crest factor
Relative $\theta$ power band	$\delta/\beta$ power ratio	Spectral flatness
Relative $\alpha$ power band	$\delta/\alpha$ power ratio	Spectral roll-off
Relative $\sigma$ power band	$\theta/\alpha$ power ratio	Spectral spread
Relative $\beta$ power band	$\alpha/\beta$ power ratio	Spectral mean*
Relative $\gamma$ power band	$\delta/(\alpha + \beta)$ power ratio	Spectral variance*
Spectral entropy	$\theta/(\alpha + \beta)$ power ratio	Spectral skewness
Renyi entropy	$\delta/(\alpha + \beta + \theta)$ power ratio	Spectral kurtosis